BACHELOR

Fluid flow in a two-dimensional model of a fungus

van Liempt, J.C.

Award date:
2017

Technische Universiteit
Eindhoven
University of Technology

Department of Applied Physics
Turbulence and Vortex Dynamics Research Group

Fluid flow in a two-dimensional model of a fungus

Bachelor Final Project

J.C. van Liempt

Supervisors:
prof.dr.ir. G.J.F. van Heijst
dr.ir. L.P.J. Kamp

R-1915-S

Eindhoven, July 2017

Abstract

In this research the influence of septa in fungi on the fluid flow is investigated. The simulations are done with COMSOL Multiphysics where the fluid is assumed to be Newtonian and incompressible. It appears that eddies are formed near the corners, Moffatt corner eddies [10]. When inertial effects become more important, so for higher Reynolds number, the time-scale at which these eddies are formed also increases. Also while for small Reynolds numbers these eddies are symmetric around the septum, for Reynolds numbers above $\mathrm{Re} = 10^{-2}$ an asymmetry starts to develop until the flow starts to behaving like a jet.

For the transport of a species diffusion is dominant over advection. Therefore a species can easily escape the eddies in the corners, so the eddies do not have an influence on the transport of the species. This means that the trapping a species in the corners is not a function of the septa. Possibly the influence of a septum on the flow has no function. However since there may be objects, like organelles and proteins, floating around in the fluid the velocity may vary when they have to pass the septum. Therefore research has to be done on the influence of these variations of the velocity on the flow. Perhaps this leads to another function of the septum.

Chapter 1

Introduction

Most fungi grow as a network of tubular, filamentous structures called hyphae. A hypha mainly grows at its tip (apice) but new hyphae can emerge by forming new tips on existing hyphae, a process called branching. The whole network is called the mycelium and shown in Figure 1.1. The hyphae of higher fungi are divided into compartments by walls with pores in it, septa, making these septate hyphae, whereas the hyphae of lower fungi are called non-septate since they do not have these septa. The distance between two septa is approximately the same for each compartment. The structure is schematically illustrated in Figure 1.2.

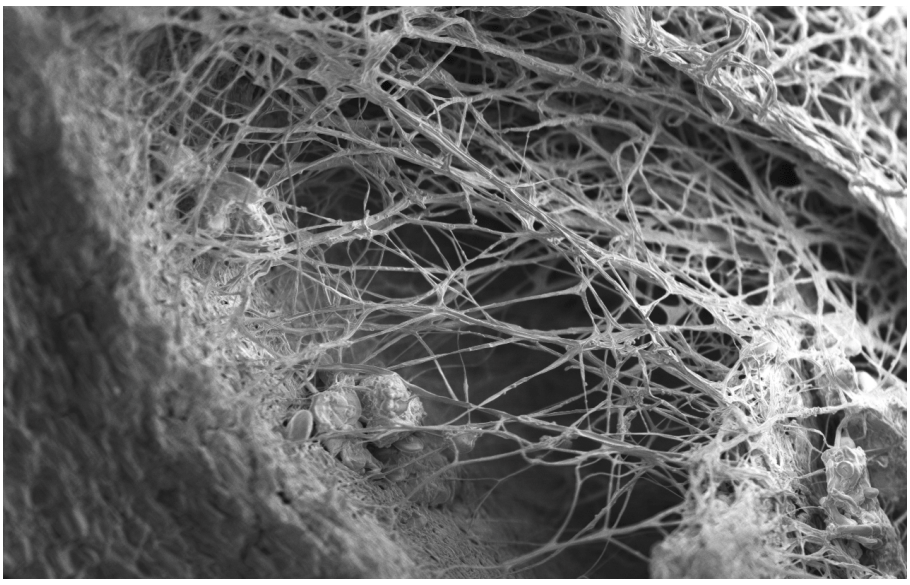

Figure 1.1: A scanning electron microscope image a bread in the bottom left corner with the mycelium of a fungus above [8].

Cytoplasm flows through the hyphae, but the pores in these septa also allow the transport of among other things organelles and proteins. In case of hyphal damage these pores can be closed in order to reduce excessive loss of cytoplasma [4]. Environmental conditions may however also trigger intact growing hyphae to plug their septa [14], which leads to heterogeneity in cytoplasmic composition in neighbouring hyphae [5]. The plugging material for the pores are called Woronin bodies.

Although much research has been done on what may trigger the septa to close, it is yet unknown

how the septa influence the flow in the hyphae. Therefore the aim of this research is to find out how these septa influence the flow in hyphae and what may be the consequences for the transport of a species.

The diameter of the pore of a septum varies between 50-500 nm and the diameter of a hypha is typically between 2-4 μm [13]. The distance between two septa can vary between 25-65 μm [4]. The bulk flow has a velocity between 3 and 70 μm/s and the kinematic viscosity of the fluid is approximately the same as for water [9]. The diffusion coefficient D_{iff} varies, depending on the species to be diffused, between $\mathcal{O}(1)$ $\mu m^2 s^{-1}$ and $\mathcal{O}(10)$ $\mu m^2 s^{-1}$. The Reynolds number is $\mathcal{O}(10^{-4})$, so the flow is assumed to be laminar [9]. Furthermore the fluid is assumed to be incompressible and Newtonian and gravity does not need to be taken into account.

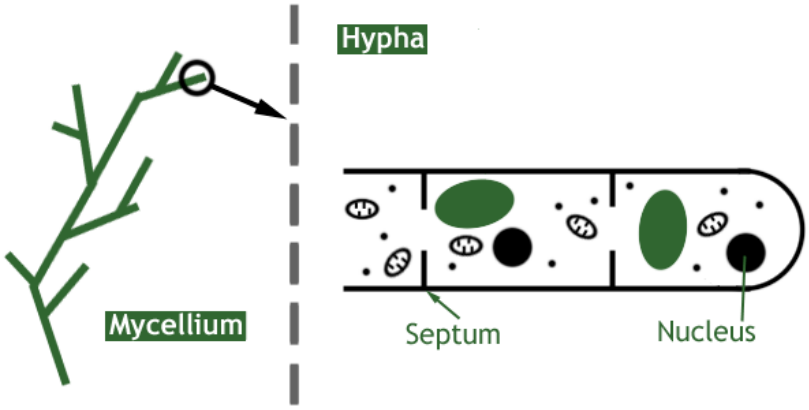

Figure 1.2: Schematic structure of a fungus. The mycellium is illustrated on the left of the dashed line, on the right the structure of a hypha is shown. In the hypha organelles are floating around in the cytoplasm [2].

Chapter 2

Problem formulation and numerical set-up

2.1 Software

All simulations will be executed in COMSOL Multiphysics, a finite element solver. Using the finite element method one can solve partial differential equations (PDE's) by defining the boundary conditions of these equations. More information about COMSOL can be found on the site [1]. The software can be used to solve several equations in a computational domain. The problem to be simulated can either be time-dependent or stationary. A stationary simulation can be used to compute the steady-state solution. Also a parametric sweep can be used where COMSOL computes the solutions for a set values of a parameter. When using a stationary simulation it is therefore useful to check whether the solutions still converge when varying the value of a parameter. The flow is assumed to be laminar, so a direct numerical solver (DNS) will be used to solve the equations without any turbulence model. The geometry of the model and the relevant equations will be elaborated in the following sections.

2.2 Geometry

The geometry of a hypha is modelled as a two-dimensional (2D) channel with septa as shown in Figure 2.1(a). H is the height of the channel, L is the length between two septa and D is the diameter of the pore in the septum. Furthermore the bulk velocity of the fluid is U and the kinematic viscosity is ν.

Now in order to make the model dimensionless, D and L are expressed in units of H, which results in the two following aspect ratios:

$$\pi_1 = \frac{D}{H} \quad \text{and} \quad \pi_2 = \frac{L}{H}. \tag{2.1}$$

Besides the channel diameter H, the bulk velocity U will also be set to 1. The dimensionless geometry is then shown in Figure 2.1(b)

In COMSOL only the top half of the geometry as shown in Figure 2.1 will be considered, so the PDE's have to be solved for only half of the geometry, which may reduce computation time. The geometry is implemented in COMSOL as shown in Figure 2.2 where the numbers denote the boundary. In this model π_1 is set to 0.05 and π_2 to 4. In reality the distance between two

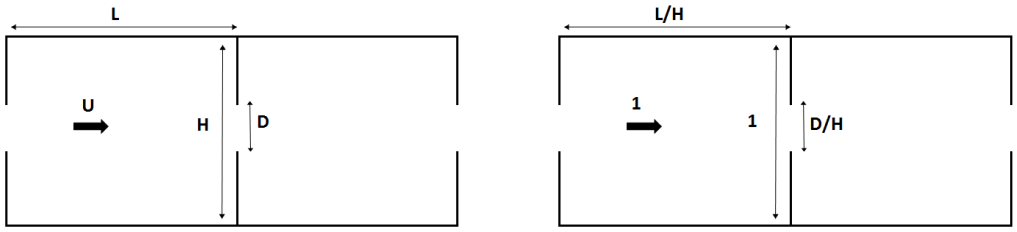

(a) L: the distance between two septa, D: the diameter of the pore, H: the height of the channel, U: the bulk velocity

(b) The geometry in its dimensionless form

Figure 2.1: Geometry of a 2D model of a hypha.

septa should be approximately 10 times bigger than the diameter of the hypha, so π_2 should be set to 10. It is however set to 4 in order to diminish computational time. The fluid enters the channel through boundary 3, and leaves it through boundary 5. Boundary 2 is the outer wall of a hypha and boundary 4 depicts the septum. The geometry is symmetric around boundary 1. The conditions applied to these boundaries depend on which equation is to be solved. The relevant equations and their boundary conditions will be discussed in the following sections.

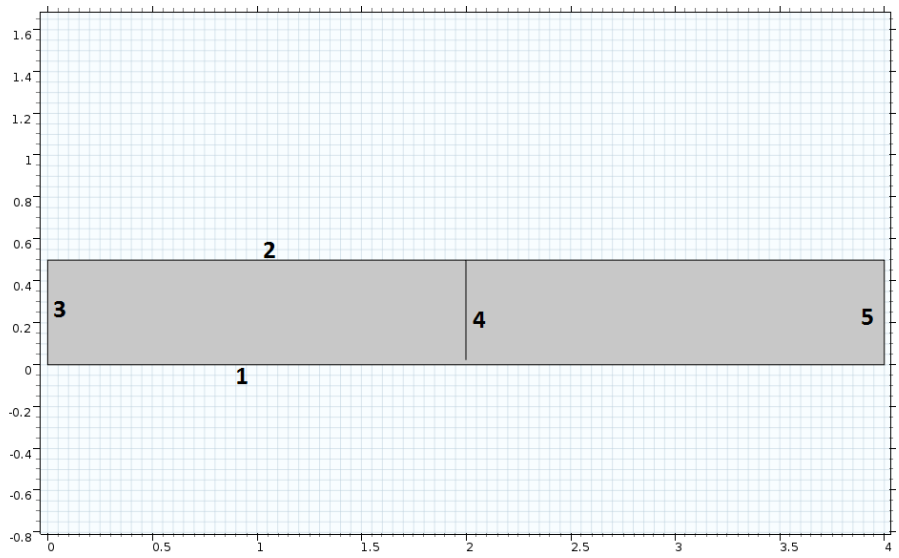

Figure 2.2: Computational domain used in COMSOL. The numbers denote the boundaries.

2.3 The Navier-Stokes equation

The fluid flow is assumed to be governed by the Navier Stokes equation for an incompressible, Newtonian fluid, which is given by

$$\rho \frac{D\mathbf{u}}{Dt} = -\nabla p + \mu \nabla^2 \mathbf{u}, \tag{2.2}$$

where ρ is the density of the fluid, $\mathbf{u}$ is the velocity vector, which consists of an x- and a y-component, p is the pressure and μ is the dynamic viscosity. Because of the incompressibility of

the fluid the divergence of the velocity is equal to zero:

$$\nabla \cdot \mathbf{u} = 0. \tag{2.3}$$

Since the geometry is made dimensionless, the Navier-Stokes equation will also be reformulated in a dimensionless form. Therefore the following dimensionless variables will be substituted in equation (2.2):

$$\mathbf{u}^* = \frac{\mathbf{u}}{U}, \quad \nabla^* = H\nabla, \qquad t^* = \frac{U}{H}t, \quad p^* = \frac{p}{\rho U^2}. \tag{2.4}$$

The dimensionless Navier-Stokes equation is then given by

$$\frac{\partial \mathbf{u}^*}{\partial t^*} + (\mathbf{u}^* \cdot \nabla^*)\mathbf{u}^* = -\nabla^* p^* + \frac{1}{\mathrm{Re}}(\nabla^*)^2 \mathbf{u}^* \tag{2.5}$$

where Re is the Reynolds number that is given by

$$\mathrm{Re} = \frac{\mathrm{UH}}{\nu}, \tag{2.6}$$

which denotes the ratio of inertial forces to viscous forces.

By solving the Navier-Stokes equation the stream lines of the flow can be calculated. These are field lines in which the tangent line is in the same direction as the velocity vector on every point.

COMSOL also provides an option to neglect the inertial term ($(\mathbf{u}^* \cdot \nabla^*)\mathbf{u}^*$=0). The resulting equation is then given by

$$\frac{\partial \mathbf{u}^*}{\partial t^*} = -\nabla p^* + \frac{1}{\mathrm{Re}}\nabla^2 \mathbf{u}^*, \tag{2.7}$$

which is called the Stokes equation and describes a Stokes flow, also called a creeping flow.

2.4 Boundary conditions for the Navier-Stokes equation

To the boundaries in Figure 2.2 the following conditions apply: to boundary 1 a symmetry condition is applied, which means that the geometry is symmetric around boundary 1 and that the fluid flows merely parallel to this boundary ($\mathbf{u} \cdot \mathbf{n} = 0$). No slip conditions are applied to boundary 2 and 4, boundary 3 is an inlet with a uniform dimensionless inflow velocity ($U = 1$) and boundary 5 is an outlet with a pressure of 0 Pa. At the outlet the backflow is suppressed.

2.5 The Poisson's equation

For the stream function ψ the following relations hold

$$u = \frac{\partial \psi}{\partial y} \quad \text{and} \quad v = -\frac{\partial \psi}{\partial x}, \tag{2.8}$$

where u is the x-component of the velocity $\mathbf{u}$ and v the y-component. In a 2D geometry the vorticity is given by

$$\omega \hat{\mathbf{z}} = \nabla \times \mathbf{u} = (\frac{\partial v}{\partial x} - \frac{\partial u}{\partial y})\hat{\mathbf{z}}. \tag{2.9}$$

This means that the following relation between the stream function ψ and vorticity ω holds

$$\nabla^2 \psi = -\omega, \tag{2.10}$$

as the Poisson's equation for the stream function, with which one can extract quantitative information about the values and positions of the streamlines. The contour lines of the stream function ψ are the stream lines so using Poisson's equation for the stream function one can select which stream lines to be plotted.

2.6 Boundary conditions for the stream function

Again the geometry in Figure 2.2 is used, but with different boundary conditions. On the boundaries 3 and 5 a zero flux condition is applied. On boundaries 2 and 4 ψ is set equal to zero using a dirichlet boundary condition. For the bottom wall 1 a value of ψ must be derived. This is done by evaluating the volumetric flow rate Q:

$$Q = \int_{\frac{H}{2}}^{H} u dy = \int_{\frac{H}{2}}^{H} \frac{\partial \psi}{\partial y} dy = \psi(H) - \psi(\frac{H}{2}). \tag{2.11}$$

For $\psi(H)$ is the value of ψ on boundary 2, this is set to 0.The velocity in the x-direction is set to 1, so equation (2.11) reduces to

$$Q = \int_{\frac{H}{2}}^{H} dy = \frac{1}{2} = -\psi(\frac{H}{2}), \tag{2.12}$$

which means that on the boundary 1 $\psi = -\frac{1}{2}$.

These boundary conditions state that at the wall $\psi = 0$, but not that the normal derivative at the wall, $\frac{\partial \psi}{\partial n}$, is zero. Both these conditions must hold at the wall, because these conditions state that the velocity at the wall is zero relative to the boundary, so another equation can be added in order to fulfil both conditions, the vorticity equation.

2.7 The vorticity equation

In order set both ψ and $\frac{\partial \psi}{\partial n}$ to zero at the wall, not only Poisson's equation will be solved, but also the vorticity equation. The voriticity is given by equation 2.9 so in order to obtain the Navier-Stokes equation in terms of vorticity, the curl of equation 2.5 will be taken:

$$\nabla \times \frac{\partial \mathbf{u}^*}{\partial t^*} + \nabla \times (\mathbf{u}^* \cdot \nabla)\mathbf{u}^* = -\nabla \times \nabla p^* + \nabla \times \frac{1}{\mathrm{Re}} \nabla^2 \mathbf{u}^*. \tag{2.13}$$

Simplifying this equation leads to the vorticity equation

$$\frac{\partial \omega}{\partial t} + \frac{\partial \psi}{\partial y}\frac{\partial \omega}{\partial x} - \frac{\partial \psi}{\partial x}\frac{\partial \omega}{\partial y} = \frac{1}{\mathrm{Re}} \nabla^2 \omega. \tag{2.14}$$

The combination of the vorticity equation and the Poisson's equation is known as the vorticity stream function formulation.

2.8 Boundary conditions for the vorticity stream function formulation

Using the boundaries as defined in Figure 2.2 the conditions are as follows. On boundary 2 and 4 $\psi = 0$, on boundary 1 $\psi = -1/2$ and on boundary 3 $\psi = y - 0.5$. On boundary 5 a zero flux boundary condition is defined, which indicates that the streamlines are perpendicular to the wall.

2.9 Diffusion equation

In order to calculate the influence of diffusion and advection on the transport of a species, the convection-diffusion equation is used, which is given by

$$\frac{\partial c}{\partial t} = D_{iff}\nabla^2 c - \mathbf{v}\cdot\nabla c, \tag{2.15}$$

where c is the concentration of the species an D_{iff} is the diffusion coefficient. Using the equation 2.4, the equation can be written down in the dimensionless form:

$$\frac{\partial c}{\partial t^*} = \frac{1}{\mathrm{Pe}}(\nabla^*)^2 c - \mathbf{v}^*\cdot\nabla^* c, \tag{2.16}$$

where Pe stands for the Peclet number, which denotes the ratio between the advective transport rate and the diffusive transport rate. This number is defined as

$$\mathrm{Pe} = \frac{\mathrm{UH}}{\mathrm{D_{iff}}}. \tag{2.17}$$

Calculating the Peclet number gives a value which ranges between $\mathcal{O}(1)$ and $\mathcal{O}(10)$.

2.10 Boundary conditions for the concentration

On the boundaries 2 and 4 zero flux conditions are defined, which means that $\mathbf{n}\cdot\nabla c = 0$ at the wall. Therefore a species cannot be transported through the wall. Through the boundaries 1, 3 and 5 a flux of a species is allowed. Furthermore an extra circular domain is placed in the model as shown in Figure 2.3. In this domain an initial concentration of a species can be defined in order to study diffusion and convection of this species and will be set to $c = 1$ in this research. In the rest of the channel, the initial concentration of this species will then be set to zero.

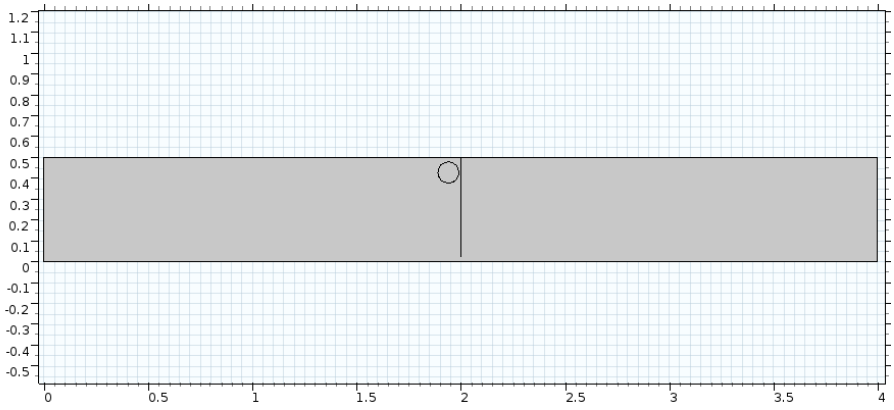

Figure 2.3: Computational domain in COMSOL with an extra circular domain

2.11 Mesh

A free triangular mesh will be used where in each triangle the PDE's are solved. Decreasing the size of these cells, thus refining the mesh, leads to a more reliable result, but more computational time is needed to solve these PDE's. Therefore when executing a simulation it is useful to find out whether the solutions change when the size of the triangles is decreased. If not time can be saved

by using a coarser mesh. When simulating a parametric sweep the size of the cells can be tested for one parameter value, the value for which the mesh is expected to need the most refined mesh, before running the whole sweep. It is expected that the most interesting region will be around the septum. Therefore an extra domain is added around the septum where the mesh can be refined without having to refine the mesh in the whole computational domain, which will probably save computation time. In Figure 2.4 an example for a mesh is shown where in the domain around the septum the mesh is much finer than in the rest of the computational domain.

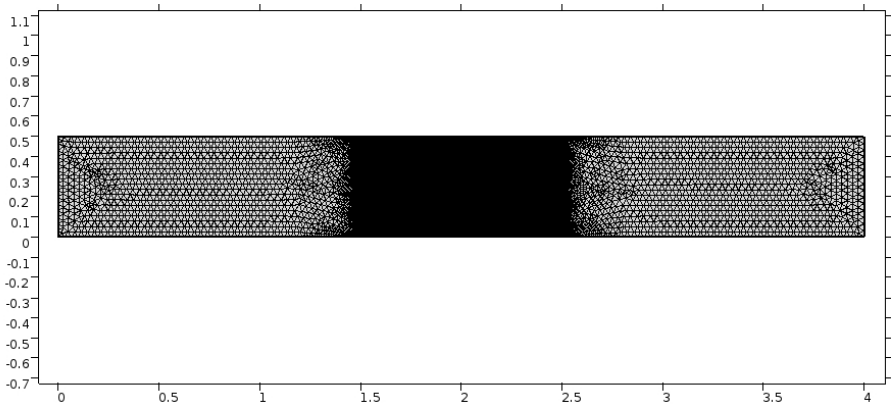

Figure 2.4: The computational domain with a free triangular mesh. In the domain around the septum the mesh is set to be extra fine, in the rest of the computational domain a coarse mesh is used.

Chapter 3

Results

3.1 Parameter values

In every simulation $\pi_1 = 0.05$, $\pi_2 = 4$ and $\mathrm{Re} = 10^{-4}$ if not stated otherwise. Also the width of the septum will be set to infinitesimally small.

3.2 Streamlines

First the dimensionless Navier-Stokes equation (equation 2.5) is solved in COMSOL in order to calculate the streamlines in a stationary flow. The result is shown in Figure 3.1.

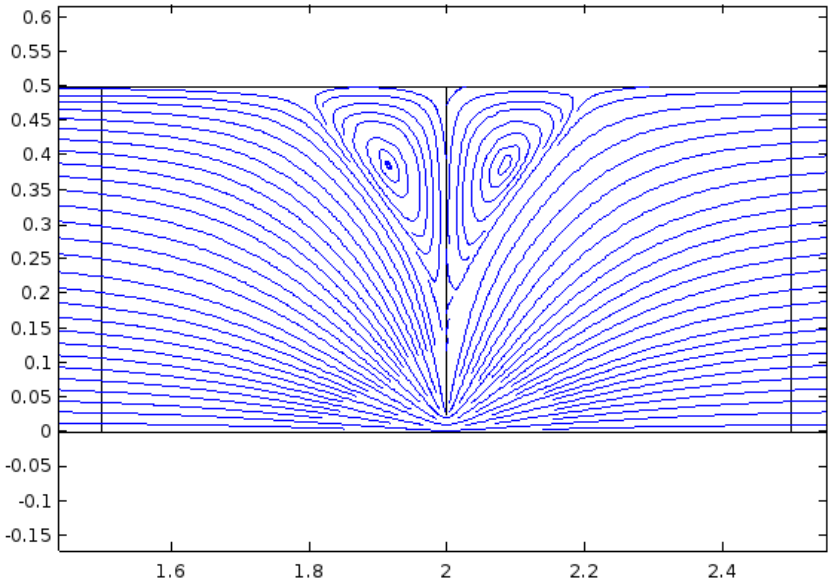

Figure 3.1: Streamlines of a flow inside a hypha.

As expected most streamlines go through the pore of the septum. In the corners between the septum and the wall however eddies can be observed. Even when neglecting the inertial term, resulting in a Stokes flow, these eddies still appear. When the density of streamlines is increased

smaller eddies appear in the corners, as is shown in Figure 3.2(a). When zooming in on the smaller eddies, the same structure can be observed as for the larger eddies (Figure 3.2(b)).

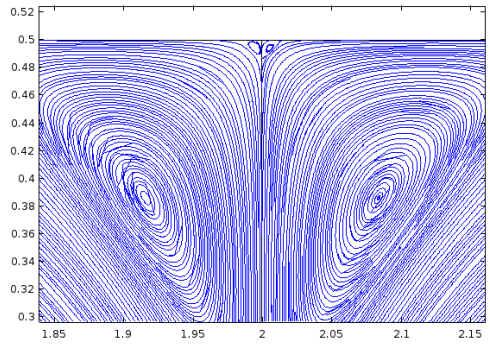

(a) In the corners between the septum and the wall smaller eddies appear.

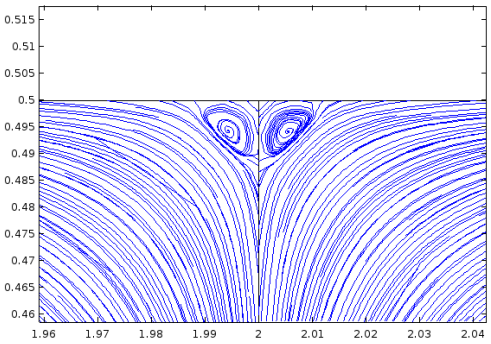

(b) Zooming in on the smaller eddies.

Figure 3.2: In the corners between the septum and the wall not only large-scale eddies appear, but also small-scale eddies.

3.3 Moffatt corner eddies

These eddies have been analysed by H.K. Moffatt [10] and appear in viscous flows near sharp corners. Also a sequence of eddies must appear near the corner. When approaching the corner, the subsequent eddies will decrease in size and intensity exponentially. This means that even smaller eddies are formed than those depicted in Figure 3.2.

3.4 Influence shape of septum

The thickness of the septum is in previous situations set to infinitesimally small. In order to justify this, the streamlines must not change when the septum has a finite thickness. The thickness of the septum is set to 0.05 and the influence of the thickness of the septum on the streamlines is shown in Figure 3.3(a). One can observe that the thickness has little influence. Also when the pore of the septum has round edges the influence is minimal as depicted in Figure 3.3(b). If the corners between the septum and the wall are round however still the corner eddies will form, but the smaller subsequent eddies will disappear (figuur 3.4).

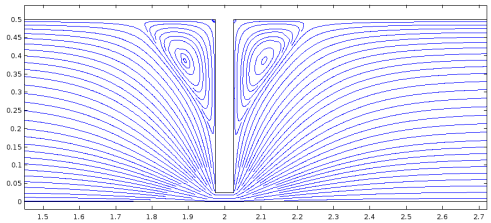

(a) Rectangular septum.

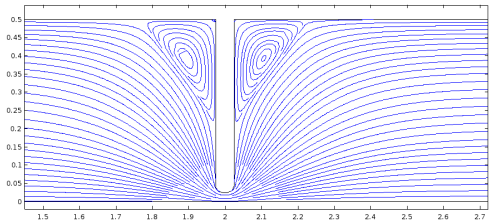

(b) Septum with rounded corners.

Figure 3.3: Influence of the shape of the septum on the streamlines.

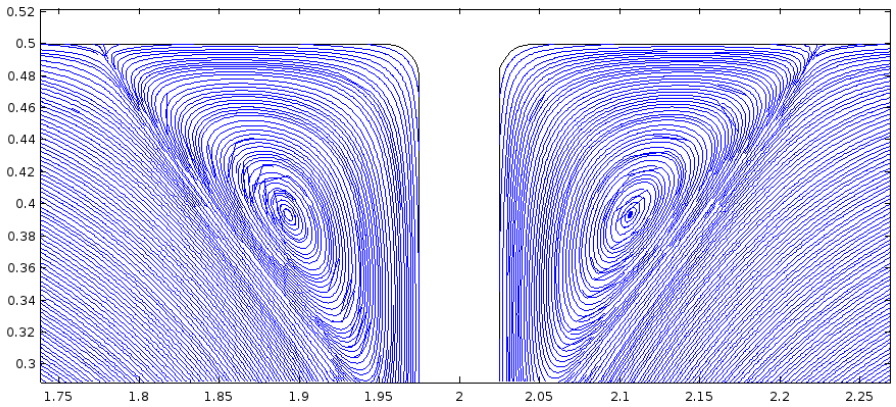

Figure 3.4: No smaller eddies appear when the corners between the septum and wall are rounded.

3.5 Influence of a septum on the flow

In these simulations the influence of previous septa on the flow is not taken into account. In order to neglect this, the distance between two septa has the be large enough so that before reaching the next septum the flow must be a fully developed Poiseuille flow. Therefore the distance from the septum at which the flow is a completely developed Poiseuille flow is searched. In Figure 3.5 de velocity magnitudes are plotted. From approximately x=2.8 a completely developed Poiseuille flow is observed. This is confirmed by Figure 3.6 which shows the velocity magnitude as a function of the channel height at x=2.8. A parabola is fitted through these points resulting in the velocity profile of a fully developed laminar Poiseuille flow. For the distance between two septa is approximately $\pi_2 = 10$, the influence of a septum on the flow profile around the next septum is negligible. This means that it is justified to simulate only the region around one septum.

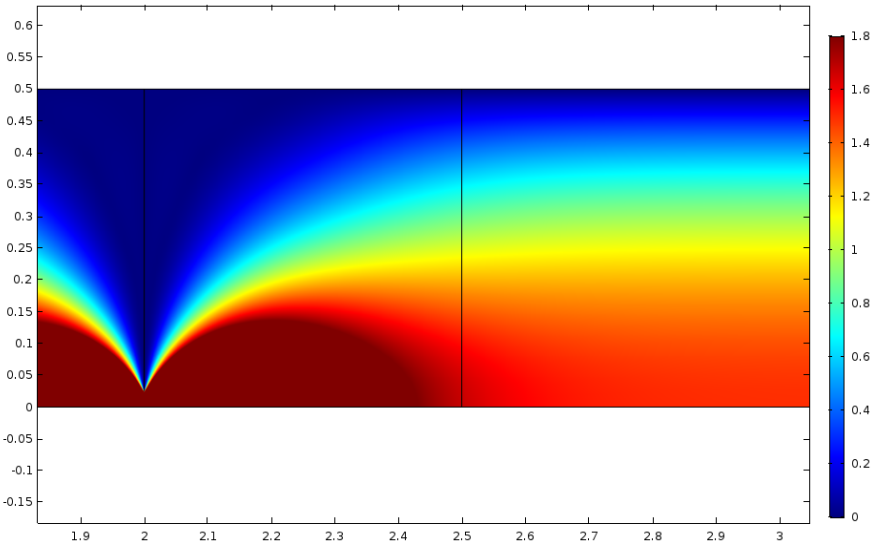

Figure 3.5: The velocity magnitudes behind a septum. The colours indicate the values of the velocity magnitude.

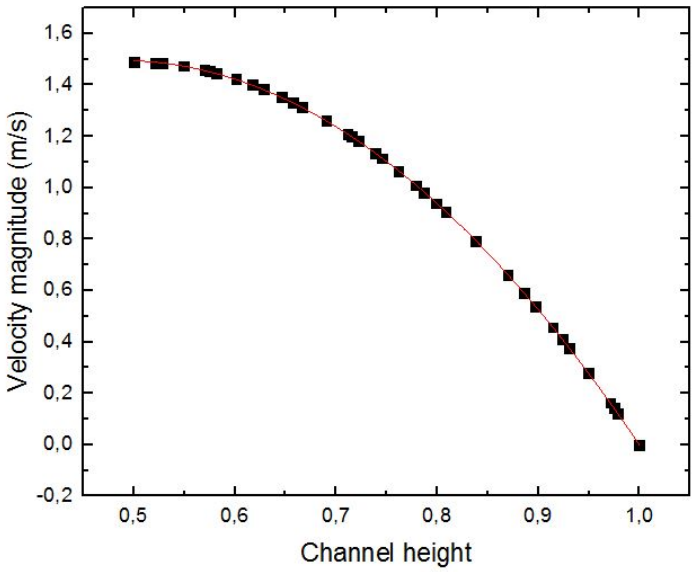

Figure 3.6: The velocity magnitude is plotted as a function of the height of the channel and a second order polynomial function is fitted through the data points.

3.6 Entrance length

In order to diminish the needed computional power only a part of the total length of a hypha is simulate, the part around the septum. In Figure 3.5 one can see that before the flow reaches the subsequent septum it is a fully developed Poiseuille flow. This means that when only simulating the region around a septum, the flow should first develop into a Poiseuille flow. The entrance length X_e, where the flow is developed in a Poiseuille flow, of a newtonian fluid in a 2D channel is given by [7]

$$X_e = [(0.631)^{1.6} + (0.0442\mathrm{Re})^{1.6}]^{1/1.6}. \tag{3.1}$$

For a channel with a Reynolds number $\mathrm{Re} = 10^{-4}$ the entrance length will be 0.613. A polynomial fit is used to analyse the velocity profile at x=0.613 in Figure 3.7. As expected the velocity profile is parabolic with a maximum in the middle of the channel which is typical for a fully developed laminar Poiseuille flow.

When working with very low Reynolds numbers (as is the case in hyphae) the second term in equation (3.1) can be neglected so the entrance length is always around x=0.6.

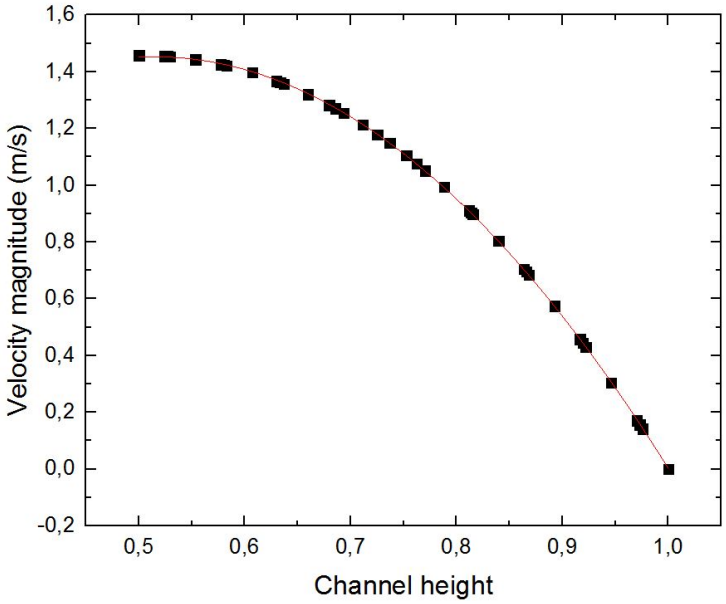

Figure 3.7: The velocity magnitude is plotted as a function of the height of the channel and a second order polynomial function is fitted through the data points.

3.7 Time-scale for development eddies

The time-scale at which corner eddies will form is studied using time-dependent simulation. It appears that an eddy is developed at approximately t=3×10^{-6}. When the simulation starts small eddies will form immediately and grow to a steady state, which can be observed in figure 3.8.

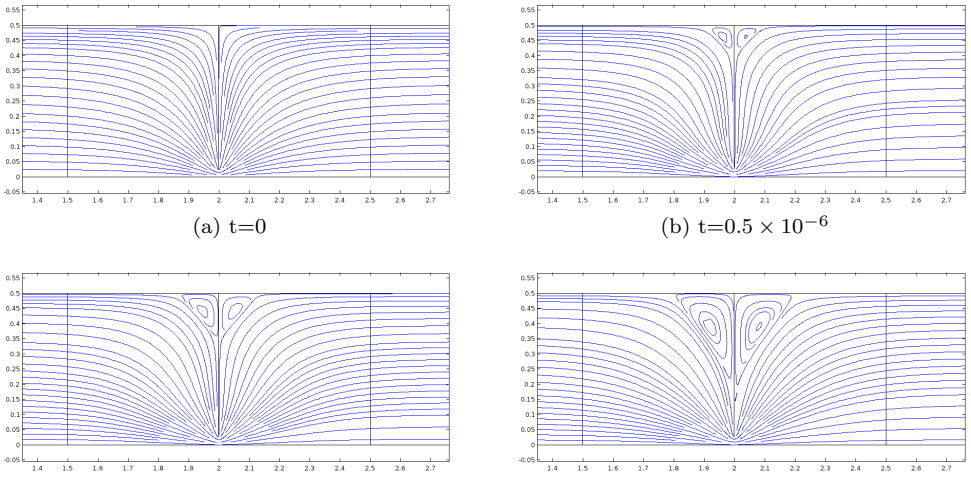

(a) t=0 (b) t=0.5 × 10^{-6}

(c) t=1 × 10^{-6} (d) t=3 × 10^{-6}

Figure 3.8: Forming of eddies, an eddy is developed at approximately t=3 × 10^{-6}.

3.8 Influence of Reynolds number

The Reynolds number is varied between Re = 10^{-8} and Re = 10. For very small values of the Reynolds number the eddies remain symmetric around the septum. However, when reaching a Reynolds number of about $\mathcal{O}(10^{-2})$ one can observe that the flow becomes asymmetric around the septum for the left eddy starts to shrink as the right eddy grows in size. This effect is shown in Figure 3.9.

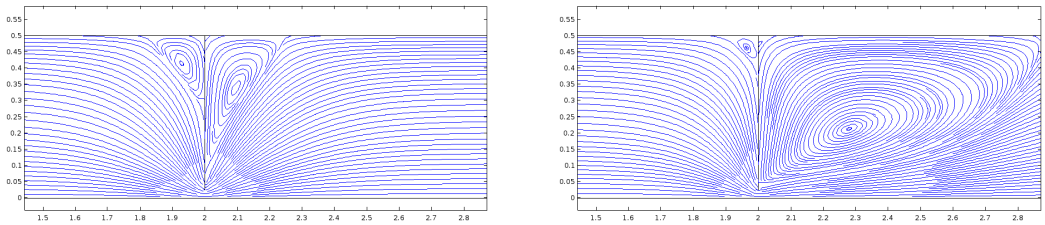

(a) Re=1 (b) Re=10

Figure 3.9: Streamlines for higher Reynolds numbers.

The positions of the stagnation points have been determined by plotting the magnitude of the velocity along four lines parallel and close to the top walls and both sides of the septum and then finding the position where the velocity is at its minimum, for the velocity should be zero at a stagnation point. The lines along which the velocities are calculated are shown in Figure 3.10.

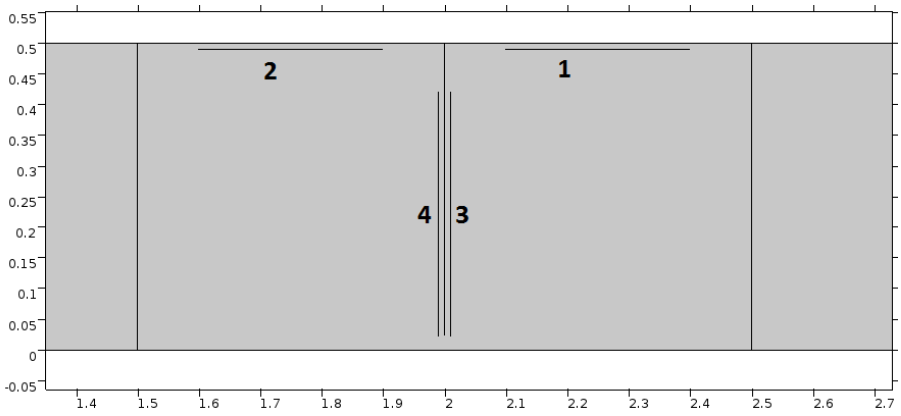

Figure 3.10: Lines along which the velocities are calculated. The numbers denote the individual lines.

The positions of the stagnation points are then plotted as a function of the Reynolds number, by using a parametric sweep over the Reynolds number, in Figure 3.11. The difference between the distances from the septum and the stagnation points on the wall remain zero until a Reynolds number of 10^{-2} is reached. From there on the difference grows, which indicates that the flow becomes asymmetric. The same holds for the stagnation points on the septum. Here an asymmetry starts to from when a Reynolds number of 10^{-2} is reached. Also the influence of the Reynolds number on the time-scale of the forming of eddies is studied. It appears that raising the Reynolds number leads to larger time-scales. While for a Reynolds number of 10^{-4} a stationary situation is reached at t=3×10^{-6} to reach a stationary situation, at t=3×10^{-5} the eddies are developed when the Reynolds number is 10^{-3}.

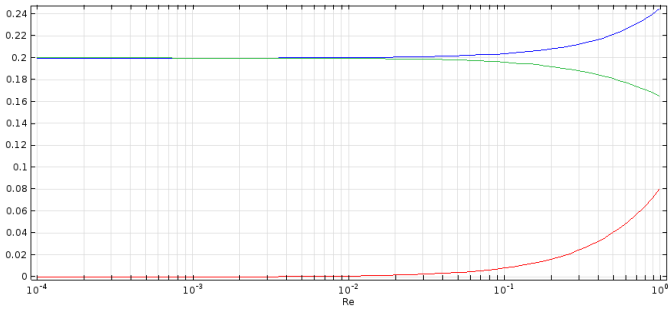

(a) The stagnation points on line 1 (blue) and line 2 (green).

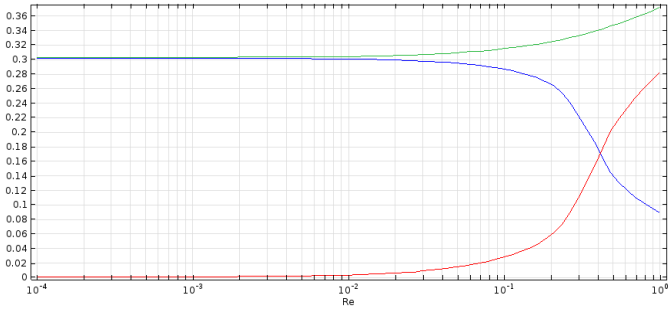

(b) The stagnation points on line 3 (blue) and line 4 (green).

Figure 3.11: The absolute distances of the stagnation points as a function of the Reynolds number from (a) the septum and (b) the wall. The blue line shows the position of the stagnation point at the right-hand side of the wall (lines 1 and 3 in Figure 3.10), the green line of the left-hand side (lines 2 and 4 in Figure 3.10), the red line shows the difference between the blue and the green line.

3.9 Influence pore diameter

The diameter of the pore is varied between $\pi_1 = 0.03$ and $\pi_1 = 0.3$. The positions of the stagnation point have been determined by the same method as in section 3.8. The positions of the stagnation points on the wall change only a little, as can be seen in Figure 3.12(a). Also the flow remains symmetric around the septum, since there is no difference in the distance from the septum to the stagnation point on the left and to the stagnation point on the right. The stagnation points on the septum do vary as the pore grows. This is logical, because if the pore grows the stagnation point also to shift. Otherwise the stagnation point would be situated in the pore in stead of on the septum.

Also the influence of the diameter of the pore on the forming of eddies has been studied using a time-depended simulation. Varying the pore diameter turns out to have very little influence on the time-scale on which the eddies develop. While for a π_2 of 0.005 a steady state is reached at t=3×10^{-6}, for a π_2 of 0.5 this is reduced to t=2.5×10^{-6}, which proves that varying the pore diameter has not only little influence on the positions of the stagnation points, but also on the time needed to develop an eddy.

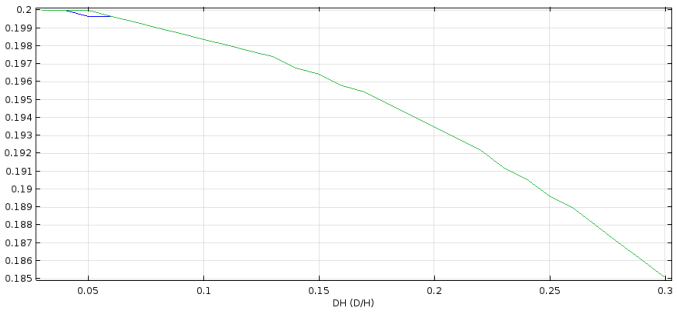

(a) The stagnation points on line 1 (blue) and line 2 (green).

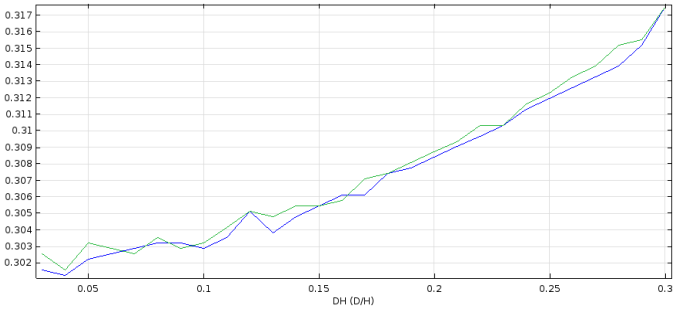

(b) The stagnation points on line 3 (blue) and line 4 (green).

Figure 3.12: The absolute distances of the stagnation points as a function of the Reynolds number from (a) the septum and (b) the wall. The blue line shows the position of the stagnation point at the right-hand side of the wall (lines 1 and 3 in Figure 3.10), the green line of the left-hand side (lines 2 and 4 in Figure 3.10).

3.10 Analysing stream lines using Poisson's equation

In the previous section an approximation of the positions of the stagnation points is made. In order to find the exact positions, the Poisson's equation (equation (2.10)) will be solved. At the wall and the septum the value of the streamline will be $\psi = 0$, so plotting this stream line should give the exact position of the stagnation point. However, when plotting this streamline the expected result is not found. In Figure 3.13 (a) the streamlines for $\psi = 0$ are plotted, but these do not give the position of the stagnation point. When plotting values of ψ approaching 0, the streamlines start to curl around the eddies. In Figure 3.13 (b) this is shown for $\psi = -3 \times 10^{-5}$. This may be due to the fact that at the wall not only ψ must be equal to zero, but also its derivative in the direction perpendicular to the wall, $\frac{\partial \psi}{\partial n}$, must be zero. Therefore the vorticity equation must be solved together with Poisson's equation to set both ψ and $\frac{\partial \psi}{\partial n}$ to zero.

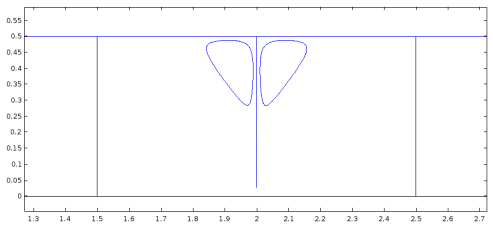

(a) $\psi = 0$

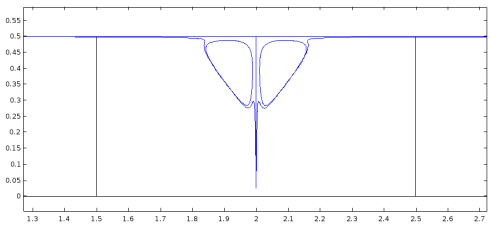

(b) $\psi = 0$ and $\psi = -3 \times 10^{-5}$

Figure 3.13: Streamlines plotted using Poisson's equation.

3.11 Analyzing streamlines using the vorticity stream function formulation

In the previous section the streamlines showed weird behaviour near the wall, presumably because the the normal derivative is not set to zero. Therefore not only Poisson's equation but also the vorticity equation (equation (2.14)) should be solved. Again the streamlines for $\psi = 0$ are plotted in Figure 3.14. The stagnation points seem to be closer to the septum than is observed in Figure 3.1. These results do not seem to be reliable, so it is no use searching for the stagnation points.

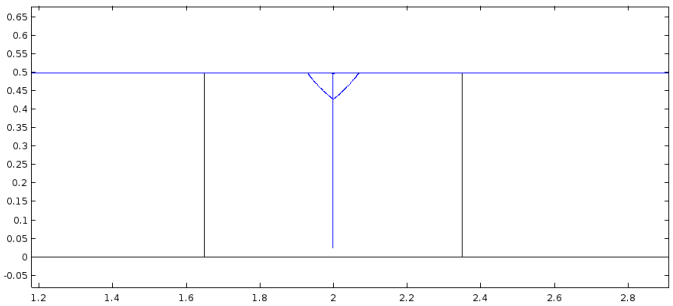

Figure 3.14: Streamlines for $\psi = 0$ found by using the vorticity equation.

3.12 Diffusion

The Moffatt corner eddies, which are studied in the previous sections, may have an influence on the distribution of a species in the flow. In order to find out whether species stay in the eddies, due to advection, or can escape these cells by diffusion the advection-diffusion equation (equation (2.16)) will be solved. The Peclet number should be $\mathcal{O}(1)$, so the first simulation is run for $\mathrm{Pe} = 1$. A species with a concentration of 1 is placed in the top left corner of a septum, while in the rest of the channel the concentration is set to 0. In Figure 3.15 (a) the concentrations of the species in the channel is shown for $\mathrm{Pe} = 1$ at $\mathrm{t}=7 \times 10^{-3}$. Also a simulation is run for a large Peclet number to see how the species will be distributed if advection has the overhand. In Figure 3.15 (b) the result is shown for $\mathrm{Pe} = 10^3$ at $t = 17$, where indeed advection has the overhand.

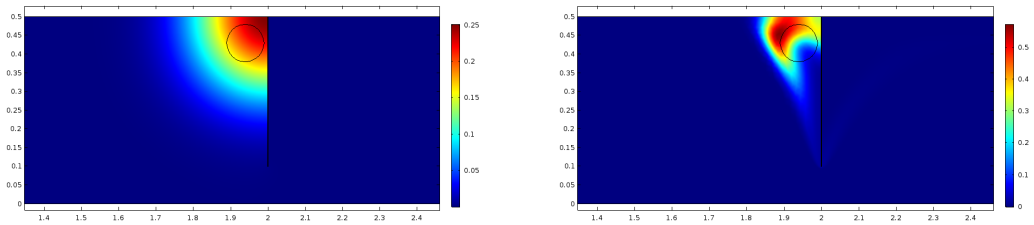

(a) Pe=1 (b) Pe=10^3

Figure 3.15: Influence of the Peclet number on transport of a species.

Chapter 4

Discussion and conclusions

The aim of this research was to gain more insight into the function of septa in hyphae, in particular its influence on the flow. Three different approaches to calculating the streamlines have been tried, which all gave different results. When solving only Poisson's equation, it is clear that it lacks one boundary condition, which makes the results unreliable. Solving the vorticity stream function formulation should fix this problem, but the results differed a lot from those when solving the Navier-Stokes equation. Taneda [12] had studied a flow with a similar geometry and found that the streamlines are similar to those when solving the Navier-Stokes equation (Figure 4.1). It is thus concluded that the streamlines calculated by using the vorticity stream function formulation are unreliable. This difference in results between the two methods can be explained by the fact that the vorticity stream function formulation has to be entered manually in COMSOL while the module for solving the Navier-Stokes equation is built in into COMSOl. This means that the solutions for the Navier-Stokes equation are stabilised, which makes these solutions more reliable than the solutions of the vorticity equation.

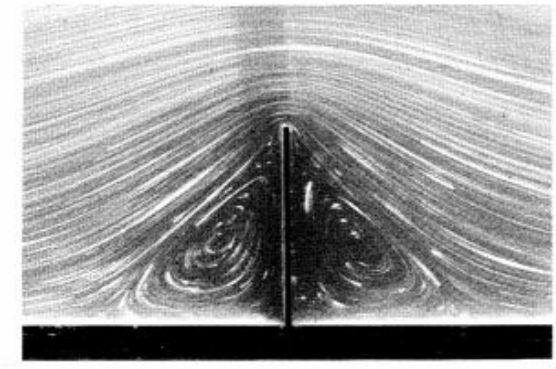

Figure 4.1: Streamline pattern of a flow past a 90°fence. ($\mathrm{Re} = 1.4 \times 10^{-2}$) [12]

Since the flow in hyphae is viscous ($\mathrm{Re} = \mathcal{O}(10^{-4})$) Moffatt eddies will form in the corners between the septa and the wall. However, the viscosity of the cytoplasm is assumed to be constant and equal to the viscosity of water, which may not be the case. By varying the Reynolds number the influence of the viscosity on the flow is simulated. The time-scale in which the eddies form is highly dependent on the Reynolds number. Raising the Reynolds ten times means that it will take ten times longer until the eddies are formed. The Reynolds number also has an influence on the sizes of the eddies. The positions of the stagnation points are analysed for parametric sweeps over the Reynolds number. While for $\mathrm{Re} = 10^{-4}$ the eddies are symmetric around the

septum, from Re = 10^{-2} the eddies start to become asymmetric, because inertial terms become more important. This means that for a viscosity a hundred times smaller than that of water the eddies become asymmetric, but this is unlikely to be the case in fungi as it should be in the same order of magnitude as that of water [9]. Furthermore the cytoplasm is assumed to be Newtonian, while it is actually a non-Newtonian fluid [6] [15] [3]. In some cases however, cytoplasm can be approximated as a Newtonian fluid [11]. It is not clear whether this is the case in fungi, but since the Reynolds number is very small, it is not expected that simulating a non-Newtonian fluid will lead to significant differences. Therefore it is concluded that the Moffatt corner eddies should be symmetric around the septum in fungi.

Since the pore diameter may vary in different septa, the influence of this diameter on the eddies is also simulated. When varying the pore diameter the eddies stay symmetric around the septum but they shrink in size as the pore grows. Also when simulating the build-up time for eddies the diameter of the pore of the septum appears to have little influence on this time-scale. However, no typical values for the width of the septum can be found in literature. Therefore it was assumed to be infinitesimally small, but in order to verify this the width was varied. In section 3.4 it is found that the width of the septum has little influence on the flow, so simulating the septum to be infinitesimally thin does not lead to unrealistic results.

The septum has a influence on the velocity profile of the flow. Therefore it was checked whether it is justified to simulate only one septum, since the influence of a previous septum may have to be taken into account. In section 3.5 it was shown that when passing a septum the flow will develop to a fully developed laminar Poiseuille flow before reaching the next septum. This means that the septa are placed in such a way that around a septum there is no influence on the flow from the previous septum. However this is only checked for a pore diameter of $\pi_1 = 0.05$. By varying the diameter, it can be checked whether this also holds for bigger and smaller pore diameters.

In section 3.12 the transport of a species was simulated for two different Peclet numbers. For Pe = 1 it turned out that the transport of a species in the corner is reigned by diffusion as little influence of the direction of the flow on the distribution of the species can be seen. When a Peclet number is equal to one, the diffusive transport is expected to be as significant as advective transport. However, velocities in the regions of the eddies are $\mathcal{O}(10^{-2})$, so the Peclet number will be much smaller in these regions, which means that diffusive transport is indeed the main transport mechanism. For Pe = 10^3 it turned out that the species is mainly distributed by the flow itself, so advection is dominant over diffusion. However, in a fungus the Peclet number is $\mathcal{O}(1)$ so the transport is reigned by diffusion. Thus, the corner eddies have no influence of the distribution of a species. Therefore it is still not clear what the function is of these eddies, if there is any. Possibly the only functions of the septum are that of preventing excessive loss of cytoplasm in case of hyphal damage and that of remaining heterogeneity in the cytoplasm as explained in Chapter 1.

However, the influence of variations in the density is not simulated. The density of the fluid is held constant in every simulation, while in the cytoplasm several object, such as organelles and proteins, float around which cause the density to vary locally. It may, for example, have a significant influence on the flow when an organelle passes through the septum, since this may slow down the flow through the septum. Simulating with a inflow velocity that varies in time may give more insight in the effect of these objects on the flow. Perhaps another function of the septum can be found when simulating the influence of these objects passing the septum.

Bibliography

[1] Comsol webiste. https://www.comsol.com/. Accessed: 26-06-2017. 3

[2] Fungi and yeast. https://scienceaid.net/biology/micro/fungiyeast.html. Accessed: 04-07-2017. 2

[3] S. Alberti. Don't go with the cytoplasmic flow. *DEVELOPMENTAL CELL*, 34(4):381–382, 2015. 19

[4] R. Bleichrodt, M. Huisman, H. A. B. Wosten, and M. J. T. Reinders. Switching from a unicellular to multicellular organization in an aspergillus niger hypha. *MBio*, 6(2):111–15, 2015. 1, 2

[5] RobertJan Bleichrodt, G. J. Veluw, Brand Recter, Junichi Maruyama, Katsuhiko Kitamoto, and Han A. B. Wsten. Hyphal heterogeneity in aspergillus oryzae is the result of dynamic closure of septa by woronin bodies. *Molecular Microbiology*, 86(6):1334–1344, 2012. 1

[6] Emil Brujan. *Cavitation in Non-Newtonian Fluids: With Biomedical and Bioengineering Applications*. Springer-Verlag, Berlin, 1st;1; edition, 2011;2010;. 19

[7] F. Durst, S. Ray, B. nsal, and O. A. Bayoumi. The development lengths of laminar pipe and channel flows. *Journal of Fluids Engineering, Transactions of the ASME*, 127(6):1154–1160, 2005. 12

[8] M. Gans. Images for eastfield college microbiology. http://murry-gans.blogspot.nl/2013/04/fungi-images-for-eastfield-college.html. Accessed: 04-07-2017. 1

[9] R. R. Lew. Mass flow and pressure-driven hyphal extension in neurospora crassa. *Microbiology*, 151(8):2685–2692, 2005. 2, 19

[10] H.K. Moffat. Viscous and resistive eddies near a sharp corner. *Journal of Fluid Mechanics*, 18(1):1–18, 1963. ii, 10

[11] Ritsuya Niwayama, Kyosuke Shinohara, and Akatsuki Kimura. Hydrodynamic property of the cytoplasm is sufficient to mediate cytoplasmic streaming in the caenorhabiditis elegans embryo. *Proceedings of the National Academy of Sciences of the United States of America*, 108(29):11900–11905, 2011. 19

[12] S. Taneda. Visualization of separating stokes flow. *Journal of the physical society of Japan*, 46(6):1935–1942, 1979. 18

[13] M. Tegelaar and H. A. B. Wosten. Apical compartments of aspergillus niger are self-sustaining in growth. h.a.b.wosten@uu.nl. 2

[14] A. F. van Peer, W. H. Muller, T. Boekhout, L. Lugones, and H. A. B. Wosten. Cytoplasmic continuity revisited: closure of septa of the filamentous fungus schizophyllum commune in response to environmental conditions. *PLoS One*, 4(6):e5977, 2009. 1

[15] Randy O. Wayne. *Plant Cell Biology: From Astronomy to Zoology.* Academic Press, US, 2009. 19